COMSOL CONFERENCE 2023 MUNICH

Towards Accurate Modelling of Aeraulic Droplets Interactions within COMSOL Multiphysics®

F. Viry[1], M. Sturma[2], P. Namy[1], B. Barbet[2]

1. SIMTEC, Grenoble, France.
2. MARKEM-Imaje, Bourg-lès-Valence, France.

Abstract

In the field of industrial marking, continuous inkjet technology is based on high speed emission of ink drops. The printing quality is directly linked to the interactions of the droplets with their environment during flight time: electric field, aerodynamic perturbations, and droplet-droplet interactions. In a former paper, all these interactions were modelled in a fully coupled Lagrangian-Eulerian approach within COMSOL Multiphysics®. Particularly, aeraulic interactions between droplets were obtained thanks to the air flow induced by all the droplets by resolving Navier-Stokes equations. Numerical simulations were compared to experimental data, showing a good agreement in terms of flight time and macroscopic position of the droplets on the printed medium but also inaccuracies in the gap between droplets, leading to a biased forecast of the printing quality. Resolving accurately the surrounding air flow requires in fact an extremely fine mesh. This paper studies another approach to take into account the aeraulic interactions between two droplets using abacuses. First, steady air flows around a unique droplet are computed using the Laminar Flow physics of COMSOL Multiphysics® for multiple droplet velocities. Second, these results are combined within interpolation functions in order to get an abacus of the air velocity field around each droplet. Finally, this abacus is integrated in the Particle Tracing physics of the former model to estimate the drag force experienced by each droplet in the air flow induced by the other one, replacing the computation of Navier-Stokes equations in the surrounding air. This new approach makes it possible to forecast phenomena of aeraulic aspiration followed by bouncing of the droplets by electrostatic repulsion, allowing a better understanding of the mechanisms and the design parameters playing on the printing quality.

Keywords: continuous inkjet printing, industrial printer, charged ink, CFD, electric field, electric interactions, aeraulic interactions, particle-particle interaction, drag force, wake.

1 Introduction

The Continuous Inkjet technology (CIJ) is based on a continuous stream of electrically charged droplets emitted at high-speed (20 m/s, 100 kHz), deflected towards their position on the printed moving media within an electric field. The printing quality depends on the interactions of the droplets with the electric field at the first order, but also on the aeraulic and electric interactions between droplets at the second order [1] [2] [3]. In former works [4] [5], all these effects were taken into account in a Lagrangian-Eulerian model within COMSOL Multiphysics®, coupling the computation of the electric field with the surrounding air flow and the dynamics of the droplets using particle tracing.

Experimental measurements have shown that there exists a minimal distance between two successive printed droplet called the *separation distance*. This distance exists because of droplets interactions, and is related to the printing resolution. The former model [5] does not predict this behavior, and requires improvements. The mesh used for fluid dynamics has been shown too coarse to resolve the wakes of each droplet, and refining the mesh was not feasible because of computation costs. This article proposes another approach using abacuses to solve accurately the aeraulic interactions between two droplets, and make the model a design support tool.

2 Experimental Set Up

a. Test Bench

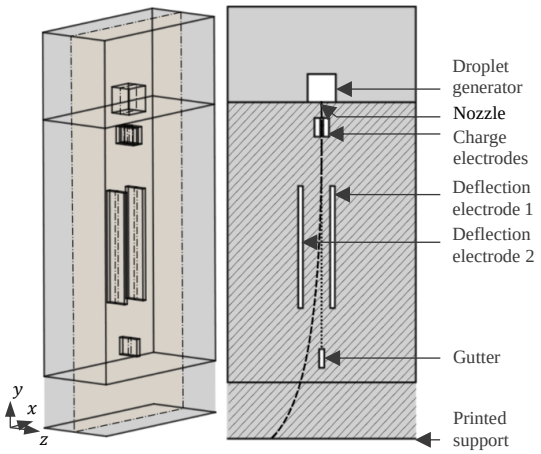

Figure 1. Plan of the print head (from [5]).

The print head is schematized in Figure 1. A stream of non-charged droplets of diameter D (*e.g.* 100 µm) and mass m (*e.g.* 1 µg) is generated by the *droplet generator* from the *nozzle* at high speed v_{jet} (*e.g.* 20 m/s) and high frequency f_{jet} (*e.g.* 100 kHz).

Then droplets pass through *charge electrodes*, whose potential difference with the ink jet make them embed a charge q (*e.g.* 1 pC), and are more or less deviated by the electric field generated by the *deflection electrodes* (Lorentz force). During their flight, each droplet interacts with each other by electrostatic repulsion (Coulomb force) and aeraulic interactions (drag force). Non-charged droplets create a wake dragging the whole droplets stream along the y-axis, and land into the gutter. Only charged droplets are printed.

The separation distance d_s is obtained as follows. Pairs of successively generated droplets having charges $q_1 = q_0$ and $q_2 = q_0 + \Delta q$ are printed. Depending on Δq, either the droplets collide each-other and their distance is $d = 0$, or the droplets are printed at distance $d \neq 0$. The distance d is measured for multiple values of Δq, and d_s is the minimal non-zero distance.

The distance d is measured optically. Each pair (q_1, q_2) is printed multiple times periodically. Droplets are enlightened using a strobe light synchronized on droplet frequency f_{jet}, and varying its phase allows to monitor droplets positions during their flight. Positions are measured using a micrometric table controller (Figure 2).

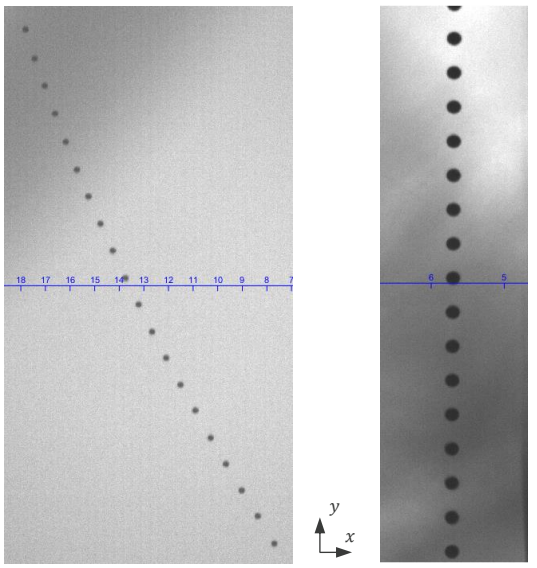

(a) Charged droplets raster deviated by the electric field in flight.

(b) Non-charged droplets in the jet axis.

Figure 2. Snapshots of positions of charged and non-charged droplets obtained on the test bench (from [5]).

b. Reference Numerical Drag Force

In order to validate the upcoming numerical approach to estimate droplet-droplet aeraulic interactions, numerical reference results for the drag force have been obtained. In this numerical experiment, two droplets are maintained close to each other with identical velocity, allowing to estimate the drag force experienced by each droplet.

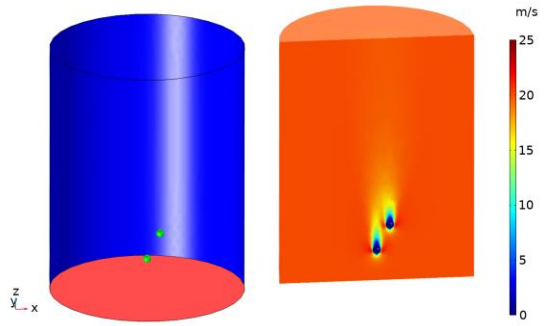

Figure 3. Numerical model to compute the reference drag force (left: geometry and boundaries; right: example of velocity field).

The air flow around the pair of droplets is modelled in the droplets frame (Figure 3), by solving the incompressible Navier-Stokes equations at steady-state using the *Laminar Flow interface*:

$$\begin{aligned} \boldsymbol{\nabla} \cdot \boldsymbol{u} &= 0, \\ \rho \boldsymbol{u} \cdot \boldsymbol{\nabla} \boldsymbol{u} &= -\boldsymbol{\nabla} \cdot (-p\mathbf{I} + \mathbf{K}), \\ \mathbf{K} &= \mu[\boldsymbol{\nabla} \boldsymbol{u} + (\boldsymbol{\nabla} \boldsymbol{u})^{\mathrm{T}}], \end{aligned} \tag{1}$$

where ρ denotes the air density, 1.20 kg/m^3, and μ the air dynamic viscosity, $1.81 \cdot 10^{-5}$ Pa · s. The boundary conditions are: air inflow at droplets velocity (Figure 3 – left: red), open boundaries (Figure 3 - left: blue), and no-slip (Figure 3 - left: green). The drag forces are computed by integrating normal stresses on each droplet:

$$\boldsymbol{F}_d = \iint (p\mathbf{I} - \mathbf{K}) \cdot \boldsymbol{n}. \tag{2}$$

The drag forces are computed on multiple configurations (relative position of the droplets, velocity), and a mesh sensitivity analysis is performed to ensure the accuracy of the results.

3 Numerical Model

a. Droplet Environing Air Flow Abacus

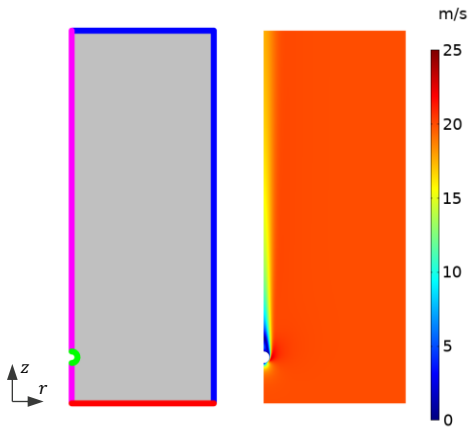

Figure 4. Numerical model of the air flow surrounding a droplet (left: geometry and boundaries; right: example of velocity field).

In the model, the aeraulic interactions between droplets are based on abacuses of the wake generated by each droplet moving in air at rest. The velocity field of the air surrounding one droplet is estimated on a 2D-axisymetric CFD model in the frame of the droplet (Figure 4).

The incompressible Navier-Stokes equations are solved at steady-state (Eq. 1) using the *Laminar Flow* interface with $\rho = 1.20$ kg/m^3 and $\mu = 1.81 \cdot 10^{-5}$ Pa · s. The boundary conditions are: air inflow at droplet velocity (Figure 4 – left: red), open boundaries (Figure 4 - left: blue), no-slip (Figure 4 - left: green), and axial symmetry (Figure 4 – left: magenta). A mesh sensitivity analysis is performed to ensure the accuracy of the results.

The velocity field is then exported as *text files* containing the radial velocity field (r, z, u_r) and the longitudinal velocity field (r, z, u_z) for multiple droplet velocities, to be integrated into the droplet dynamics model.

b. Electric Field and Droplet Dynamics

The trajectories of two droplets are solved in the 3D geometry of the print head (Figure 1). This section follows partially section 3.3 of [5].

The electric field is controlled by the potential differences between deflection electrodes (*e.g.* 1 kV), but also each conductive part of the head. It is numerically obtained by solving the Laplace equation in air using the *Electrostatics interface*:

$$\Delta V = 0. \tag{3}$$

The electric field is then obtained as follows:

$$\boldsymbol{E} = -\boldsymbol{\nabla} V. \tag{4}$$

The dynamics of the droplets is modelled in a Lagrangian approach using the *Particle Tracing for Fluid Flow interface*, through the fundamental principle of dynamics:

$$m\,\frac{d\boldsymbol{v}_i}{dt} = \boldsymbol{F}_l(i) + \boldsymbol{F}_c(i) + \boldsymbol{F}_g(i) + \boldsymbol{F}_d(i), \qquad \boldsymbol{v}_i = \frac{d\boldsymbol{x}_i}{dt}, \tag{5}$$

where i is the index of the considered droplet, $\boldsymbol{x}_i$ is its position, $\boldsymbol{v}_i$ is its velocity, $\boldsymbol{F}_l$ models the droplet-electric field interaction through the Lorentz force:

$$\boldsymbol{F}_l(i) = q_i\,\boldsymbol{E}(\boldsymbol{x}_i), \tag{6}$$

$\boldsymbol{F}_c$ models the electrical droplet-droplet interaction through the Coulomb force:

$$\boldsymbol{F}_c(i) = \frac{1}{4\pi\varepsilon_0}\sum_{j=1}^{N} q_i\,q_j\,\frac{\boldsymbol{x}_i - \boldsymbol{x}_j}{\left|\boldsymbol{x}_i - \boldsymbol{x}_j\right|^3}, \tag{7}$$

$\boldsymbol{F}_g$ is the gravity force, which can be neglected because of the lightness of the droplets, and $\boldsymbol{F}_d$ models the aeraulic droplet-droplet interaction as a drag force:

$$\boldsymbol{F}_d(i) = f(i)\cdot(\boldsymbol{u}_i - \boldsymbol{v}_i), \tag{8}$$

where $\boldsymbol{u}_i$ is the air velocity at experienced by droplet i at its position, and f is a friction coefficient given by the Schiller-Naumann drag law [6], adapted for the range of Reynolds number encountered in this process (up to $10^2 - 10^3$):

$$f(i) = 3\,\pi\,\mu\,D\,(1 + 0.15\cdot[R_e(i)]^{0.687}), \qquad R_e(i) = \frac{\rho\,D\,|\boldsymbol{u}_i - \boldsymbol{v}_i|}{\mu}. \tag{9}$$

The novelty of this work is using precomputed values for $\boldsymbol{u}_i$. Physically, the air inside the print head is initially static. Once the two droplets are propelled, the air is locally perturbed and a wake is created backwards each droplet. In the model, droplet i experiences a specific velocity field generated by the wake $\hat{\boldsymbol{u}}_j$ of the other droplet j:

$$\boldsymbol{u}_i = \hat{\boldsymbol{u}}_j(\boldsymbol{x}_i) \tag{10}$$

Precisely, $\hat{\boldsymbol{u}}_j$ designates the steady-state air velocity field around droplet j with static air in front of it. This velocity field is obtained from abacuses constructed in subsection a, by performing a change of frame such that:

$$\hat{\boldsymbol{u}}_j(\boldsymbol{x}_j) = \boldsymbol{v}_j, \tag{11}$$

Source z-axis targets destination $-\boldsymbol{v}_j$ axis.

This way, the precomputed velocity field at subsection a is mapped into the print head model.

In the physical process, the charged and non-charged droplets are generated near downstream the nozzle at velocity v_{jet} at frequency f_{jet}, and are dragged towards the gutter by the stream of non-charged droplets. Since this model does not take into account non-charged droplets, the two modelled charged droplets are dropped initially in the region where they leave the stream of non-charged droplets, with initial velocity equaling the stream velocity [5], in order to reduce position and velocity biases.

c. Numerical Aspects

The electric field is solved on the same mesh than in [5]. V is discretized with $P2$-elements. The

numerical problem is linear and takes less than one minute to solve 1 million DOFs on recent laptop.

The droplet trajectories are solved using a generalized-α solver, with a constraint on the maximal time step, in order to solve finely electrical and aeraulic interactions. The numerical problem solves 6 DOFs in a few minutes.

The abacuses of velocity field are built using the *Interpolation function* feature, allowing to import and interpolate d-dimensional point clouds. The velocity field at a specific droplet velocity is obtained by interpolation between precomputed droplet velocities. The change of frame is implemented using the *Analytic function* feature.

4 Results and Discussion

a. Drag Force

The drag force obtained in the droplet trajectory model using Eq. 8-9 is compared with the reference model described in section 2.b for three relative placement of the droplets (Figure 5) at velocity 20 m/s. The Reynolds number goes up to 200.

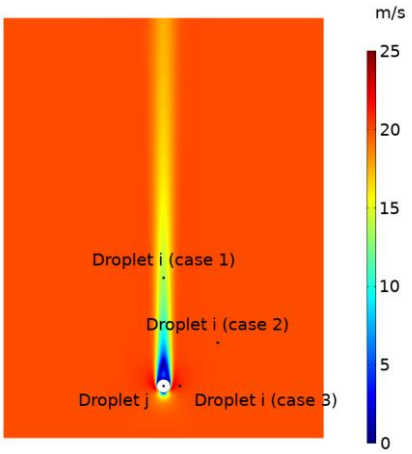

Figure 5. Velocity field in the vicinity of droplet j (at 20 m/s) used to estimate the drag force of droplet i at different locations.

Table 1. Numerical and reference radial and vertical drag force results.

Case		Reference (µN)	Model (µN)
1	Radial	0	0
	Vertical	1.88	1.31
2	Radial	0	0
	Vertical	2.45	2.43
3	Radial	0.31	0.03
	Vertical	2.75	2.57

The numerical results are given in Table 1. In case 1, droplet i experiences aeraulic aspiration - more precisely less drag - because it lies in the wake of droplet j. The numerical model predicts the right order of magnitude for the drag force, while the norm of the force is slightly underestimated. In case 2, droplet i is far from droplet j, experiencing a drag force due to its interaction with air at rest. The numerical model is very accurate in this case. In case 3, droplet i trajectory is parallel with droplet j's one, while droplets are close enough to interact with each other through the boundary layer developing around each one. The numerical model predicts aeraulic repulsion along the radial axis but underestimates it. The vertical component is accurately predicted. These results confirm the relevance of using an abacus for the velocity field around one droplet, and the Schiller-Naumann drag law, to estimate the drag force experienced by the other droplet.

b. Two-Droplets Charge-Distance Behavior

Results of the experiment described in section 2.a are illustrated in Figure 6, for some charge q_0 given at charging potential $V_0 = 210$ V. When the difference of charging potentials ΔV is below 7.2 V, the droplets collide and $d = 0$. Between 7.2 V and 9.2 V, d is highly nonlinear, certainly because of aeraulic and electrostatic interactions. Above 9.2 V, d becomes linear. The separation distance is $d_s = 530\ \mu m$.

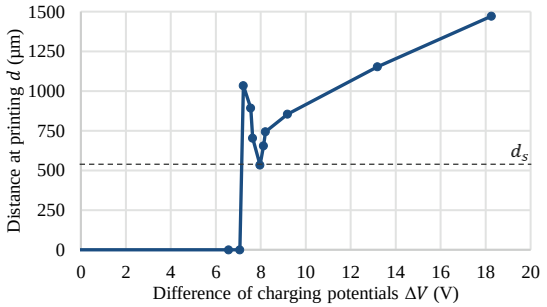

Figure 6. Experimental results of the two-droplets charge-distance behavior.

Figure 7 illustrates the results obtained using the numerical model for charge $q_0 = 1.55$ pC (charge obtained from an empirical law for $V_0 = 210$ V). Below 0.12 pC, droplets collide and $d = 0$. Between 0.12 pC and 0.26 pC, d is nonlinear. Above 0.26 pC, d is linear. The separation distance is $d_s = 2500\ \mu m$.

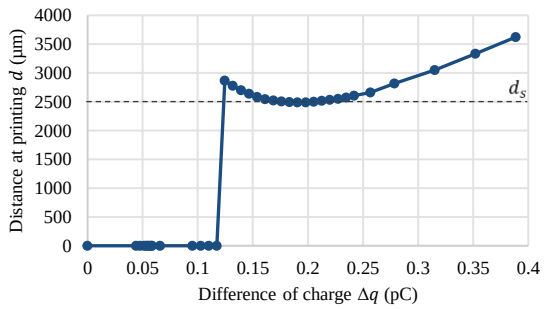

Figure 7. Numerical results of the two-droplets charge-distance behavior.

The numerical model reproduces qualitatively the experimental behavior when increasing Δq: collisions, d nonlinear and existence of a minimal

value d_s, and d linear. When Δq is low, droplets stay roughly on the same trajectory, and attract intensively each other by aeraulic aspiration, resulting in their collision. When increasing Δq, the trajectory of the second droplet slightly deviates from the trajectory of the first one, decreasing aeraulic interactions. When Δq exceeds a threshold, electrostatic repulsion becomes more important than aeraulic aspiration, resulting in a local maximum for d. Increasing Δq increases the distance between droplets in flight, reducing the work of electrostatic repulsion. In the linear regime, d is mainly due to effect of the electric field generated by deflection electrodes. The model is then helpful to explain the physical mechanisms behind the nonlinear behavior of d, and the separation distance.

Quantitatively, the numerical model overestimates the separation distance d_s, which is consistent with the fact that the numerical drag force is slightly underestimated (section 4.a), preventing droplets from being as close as possible. Moreover, charged droplets are released in the area where they may leave the stream of non-charged droplets, which is in fact a large area, revealing uncertainties on the initial state of the droplets, and resulting in uncertainties on d.

A drawback of this approach is its difficulty to extend to the interactions of more than two droplets because of the nonlinearities of Navier-Stokes equations for the values of the Reynolds number encountered ($10^2 - 10^3$).

Still, this model is a major improvement of previous models [4] [5] thanks to its qualitative results, allowing to explore numerically the levers to optimize the printing resolution.

5 Conclusions

In CIJ printing, aeraulic and electrostatic interactions between droplets must be understood and quantified in order to assess numerically the printing quality. An existing numerical model for the trajectory of droplets in CIJ printing has been improved in order to increase the accuracy of aeraulic interactions. The novelty of this work is using the Schiller-Naumann drag law with precomputed air velocity fields to obtain an adequate estimation of the drag force. This model only simulates the trajectory of two droplets.

The accuracy of the drag force computation has been assessed by comparing it with results of a reference model, showing both the relevance of the Schiller-Naumann drag law and the approach. The numerical model has been used to reproduce an experiment assessing the minimal distance between two successive printed droplets. The numerical model retrieves qualitatively the experimental behavior, which goes beyond the former works.

This model has been used as a design support tool, allowing to understand levers having an importance on the printing quality. Future works will be dedicated to the improvement of the quantitative predictability of the model, and the extension to more droplets.

References

[1] G. D. Martin, S. D. Hoath and I. M. Hutchings, "Inkjet Printing - The Physics of Manipulating Liquid jets and Drops," *Journal of Physics: Conference Series*, vol. 105, 2008.

[2] M. Ikegawa, I. Eiji, N. Harada and T. Takagishi, "Development of Ink-Particle Flight Simulation for Continuous Inkjet Printer," *Journal of Manufacturing Science and Engineering*, vol. 136, no. 5, 2014.

[3] S. Matsumoto, T. Inoue and J. Matsuno, "Flight Stability of Droplets in an Electrostatic Ink-Jet Printer," *Recent Progress in Ink Jet Technologies II*, pp. 280-285, 1999.

[4] M. Sturma, P. Namy, V. Bruyère and B. Barbet, "Modeling of charged droplet dynamics in an Electric Field using COMSOL Multiphysics®," in *COMSOL Conference 2020 Europe*, 2020.

[5] F. Viry, M. Sturma, P. Namy and B. Barbet, "Electrostatic and Aerodynamic Modelling of the Charged Droplet Trajectories thanks to a Lagrangian-Eulerian Model in COMSOL Multiphysics®," in *19th International Multidisciplinary Modeling & Simulation Multiconference*, Rome, 2022.

[6] COMSOL, "Other Drag Laws, Schiller-Naumann," in *Particle Tracing Module, User's Guide, COMSOL 5.6*, 2020, p. 270.

Acknowledgements

This work has been founded by MARKEM-Imaje and made in a fruitful collaboration between MARKEM-Imaje and SIMTEC.